Chapter 2
Creep-Damage Processes in Cyclic Loaded Double Walled Structures

Holm Altenbach, Dmytro Breslavsky, and Oksana Tatarinova

Abstract The paper presents an approach to determining the level of creep deformation and long-term strength of structural elements that operate under conditions of cyclic loading and heating. The method for solving the boundary - initial value problem is described. It is based on the combination of FEM and difference methods of integration for initial problems. The basis of the method is the developed and verified constitutive equations for modeling the cyclic creep-damage processes in the material. The main feature of the method is the transformation of the initial cyclic problem to a new at uniform loading and heating, but with constitutive equations of developed type. The case of the cycle stresses varying in a wide range, including in the conditions where they exceed the yield stress, as well as the case of creep when it is not exceeded by stresses, are considered. The numerical model of double-walled blade is considered and different cyclic creep modes of its operation were analyzed.

2.1 Introduction

Creep processes, which are accompanied by the accumulation of hidden damage, significantly limit the lifetime of various structural elements operating in high-temperature fields and high pressures. First of all, this applies to power machines, such as steam and gas turbines, gas turbine engines (GTE) etc. The modes of operation of their structural elements, leading to a complex form of boundary conditions, as

Holm Altenbach
Lehrstuhl für Technische Mechanik, Institut für Mechanik, Fakultät für Maschinenbau, Otto-von-Guericke-Universität Magdeburg, Universitätsplatz 2, 39106 Magdeburg, Germany,
e-mail: holm.altenbach@ovgu.de

Dmytro Breslavsky · Oksana Tatarinova
Department of Computer Modelling of Processes and Systems, National Technical University "Kharkiv Polytechnic Institute", UKR-61002, Kharkiv, Ukraine,
e-mail: dmytro.breslavsky@khpi.edu.ua,ok.tatarinova@gmail.com

H. Altenbach and K. Naumenko (eds.), *Creep in Structures VI*,
Advanced Structured Materials 194, https://doi.org/10.1007/978-3-031-39070-8_2

well as the very complex geometric shape of these elements, led to the need to use numerical methods of calculation, primarily the Finite Element Method (FEM). By now, approaches and methods of FE analysis of creep under a complex stress state, implemented in modern versions of engineering calculation systems, can already be considered satisfactorily developed.

Methods for numerical FE analysis of creep-damage processes, as well as of the development of macroscopic defects resulting from the long-term action of these processes, are also being developed quite successfully [1–5], although they have not yet become standard for engineers. This is largely due to the complexity of constructing the defining constitutive and evolution equations, and, most importantly, obtaining the constants that are included in them, followed by verification of the resulting relationships. The choice of approach - the use of a scalar or tensor expression for the damage parameter also either limits the possibility of a more adequate description of the process of defect development in the material, or requires a very large amount of expensive and lengthy experimental investigations.

Recent years have been characterized by increased interest in the use of cooled blades operating at elevated temperatures in gas turbine engines (GTE). It is noted that double wall transpiration cooling (DWTC) systems allow to increase the operating temperature of gas turbines in comparison with a further increase in engine efficiency [6]. Creep calculations and analysis of the long-term strength of cooled and double-walled blades continue to be the focus of researchers [7–13].

Today thermomechanical stresses are one of the most serious problems in the implementation of these systems, and they must be taken into account, along with aerothermic characteristics, at the initial stages of design [8]. With the help of the proposed computational method, which combines both parts of the analysis, the modelling of the long-term behavior of double walled blades was performed. The calculated temperature distribution was used in thermomechanical FEA to determine the stresses in the double wall under thermal loading.

The fracture of aviation turbine blades at high temperatures was studied in [7]. Constitutive creep equations with temperature interpolation are constructed, and heat transfer is analyzed. The deformed state of the blade before failure is analyzed. The creep fracture time of the blades is determined to be 91 hours.

According to the data presented in [9], it can be concluded, that temperature differences have a greater impact on the service life of the blade than pressure differences. In [13], the effect of holes on the creep of samples with holes simulating a cooling blade was investigated. It was shown that the creep term was longer in thin-walled specimens with one central hole and shorter in specimens with multiple holes due to their interaction.

In [10–12], an analysis of the typical behavior of a cooled turbine blade was performed. The authors used an original approach in which the complex three-dimensional design of the turbomachine blade is represented by simplified two -and one dimensional models. The possibilities of analytical solution for the problem components, which represent such nonlinear deformation processes, as plasticity, ratchetting, creep, etc., were used.

GTE blades used on vehicles operate under conditions of complex temperature-force cyclic loading. For such conditions of their operation, it is known [14] that the supposition of varying components on constant load values or temperatures can significantly increase the creep rate and damage accumulation in the material. In this regard, the problem of an adequate description of the processes of cyclic deformation continues to be relevant [15–22].

Cyclic deformation processes are more complex than static ones. In this regard, experimental studies are carried out to construct constitutive equations for the description of cyclic deformation and to understand the processes taking place in the material. The processes of the interaction of creep and low-cycle fatigue are studied [15, 17] and the dependence of the main values on the strain, the strain rate, static recovery and the average stress ranges were experimentally verified [15]. The effects of previous cyclic loading on the creep of steel were studied [22]. For the case of the interaction of creep and cyclic plasticity, data on the change in the slope of the "creep strain rate - stress" curve when a certain stress value is reached, were determined [19]. For static load conditions with cyclic fatigue, the process of stress relaxation was studied [21]. Cyclic strengthening processes were studied, the influence of maximum plastic deformation due to preloading and ratcheting was analyzed [20].

The experimental results obtained in these and other studies are used to formulate and verify the constitutive equations to reflect all the main effects that occur during cyclic deformation - creep, plasticity, strengthening, damage, etc. The approaches of continuum mechanics and continuum damage mechanics, models of Hayhurst [22], Chaboche [14–16, 23], physical based and micromechanical models [17, 18, 21] are used now. The built constitutive equations are used in the simulation of a complex stress state in FEA.

The presented paper contains a description of the calculation method and constitutive equations for creep-damage processes under cyclic loads and heating, which is used for the analysis of a simplified DWTC system model. The large number of cooling channels and the complex geometric shape of the blades lead to the fact that direct numerical analysis often cannot be satisfactorily applied to elucidate the qualitative patterns of their deformation and damage accumulation leading to fracture. In this regard, a simplified two-dimensional model, includes a number of typical DWTC system operating modes are considered. FEM was used for numerical modeling, which allows transferring all the main approaches and algorithms to a general three-dimensional model.

2.2 Constitutive Equations

To carry out computational studies of creep using FE approaches, it is necessary to use creep-damage constitutive equations, as well as plasticity at the stages of forcing engines, which can be implemented to the general method and algorithms that support it. The incremental theories of creep and plasticity are used.

2.2.1 Static Loading

To determine plastic strains, we apply the flow rule with isotropic hardening [24] and use the Huber-von Mises plasticity condition:

$$f\left(\sigma_{ij}\right) = \frac{3}{2} S_{ij} S_{ij} - \left[\Phi\left(\int dp_i\right)\right]^2 \tag{2.1}$$

where

$$S_{ij} = \sigma_{ij} - \delta_{ij}\sigma_{ii}$$

are the components of stress deviator,

$$\int dp_i$$

is the Odquist parameter, σ_v is von Mises equivalent stress. In this case, the components of plastic strain ε_{ij}^p increments are determined as follows:

$$d\varepsilon_{ij}^p = \frac{3}{2}\frac{dp_i}{\sigma_v} S_{ij}. \tag{2.2}$$

Classical creep-damage laws (strain hardening or Norton creep, Kachanov-Rabotnov damage equation for scalar parameter, Arrhenius-type temperature function [3, 24]) are used

$$\dot{c}_{ij} = \frac{3}{2} B c_{vM}^{-\alpha} \frac{(\sigma_v)^{n-1}}{(1-\omega)^l} \exp\left(-\frac{Q_c}{T}\right) S_{ij};\ \ Q_c = \frac{U_c}{R}; \tag{2.3}$$

$$\dot{\omega} = D \frac{(\sigma_{vd})^m}{(1-\omega)^l} \exp\left(-\frac{Q_d}{T}\right);\ \ Q_d = \frac{U_d}{R}. \tag{2.4}$$

Here c_{ij} are the components of creep strain tensor, c_{vM} is von Mises equivalent creep strain, U_c, U_d are the values of activation energies for creep and creep damage accumulation processes, R is universal constant. σ_{vd} is equivalent stress has to be estimated by use of strength criteria at the step of governing the conditions of hidden damage accumulation finishing. As is known [3], the values of material constants B, D, n, m, l, α included in (2.3) – (2.4), can be obtained by use of experimental data processing.

2.2.2 Cyclic Loading. Stresses Lower the Yield Limit

Let us consider the main equations for the case of cyclic varying of temperatures and stresses. In this case, by cyclicity we understand the alternation of long periods of gas turbine or turbine operation (hours in the first case and months in the other) with stop periods. We will demonstrate it by a simplified dependence of temperature and

stress on time (Fig. 2.1), in which we neglect the regions of increase and decrease. Here t_1 is the operating time, t_2 is the dwell time. Further, in this approximation, we consider the periods T_c, defined as $T_c = t_1 + t_2$, to be the same for the entire time of further operation. In fact, the rectangular approximation is often quite sufficient, since the integration operation (see below) is used to obtain the equations, and the value of the corresponding area under the curve is decisive.

Let us use the constitutive equations (2.3) – (2.4), and for the sake of simplicity we use Norton's law and assume $\alpha = 0$. To perform an analysis of the behavior of structural elements operating under a complex stress state, it is first necessary to analyze the one-dimensional behavior of the materials from which they are made. Behavior patterns obtained at the same time can also be detected when solving two- and three-dimensional problems, which will facilitate their analysis.

First, we consider the one-dimensional case with the action of tension stress σ^u . For the case of stress cycling, it can be represented by the sum of constant σ and time-varying components σ^1: $\sigma^u = \sigma + \sigma^1$. Similarly, the temperature function has a constant part T and periodically varying T_1: $\tilde{T} = T + T_1$. The law of cyclic varying for above stress is represented by a polyharmonic law with a period T_p:

$$\sigma^u = \sigma + \sigma^1 = \sigma\left(1 + \sum_{k=1}^{\infty} M_k \sin\left(\frac{2\pi k}{T_p} t + \beta_k^{\sigma}\right)\right) \tag{2.5}$$

where $M_k = \dfrac{\sigma_{ak}}{\sigma}$, σ_{ak} are the coefficients of stress function σ_1 expansions into Fourier series. First, we will assume that the temperature has a constant value T and the exponential factor in (2.3) – (2.4) will be equal to 1. We will expand the creep strain and damage parameter functions into an asymptotic series with a small parameter

$$\mu = \frac{T_p}{t_*},$$

where t_* is the time of finishing the hidden damage accumulation. We limit ourselves to two terms of the these series, which is the usual procedure of asymptotic methods [25, 26]:

$$c \cong c^{(0)}(t) + \mu c^{(1)}(\xi); \;\; \omega \cong \omega^{(0)}(t) + \mu\omega^{(1)}(\xi) \tag{2.6}$$

where $c^{(0)}(t), \omega^0(t), c^{(1)}(\xi), \omega^{(1)}(\xi)$ are the functions which reflect creep and damage processes in slow time (0) and fast time (1). Here we consider two time variables:

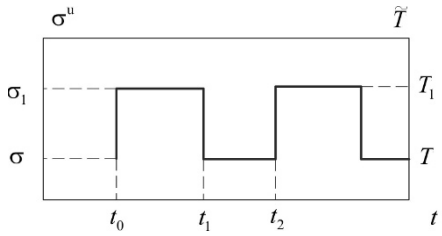

Fig. 2.1 Representation of simplified temperature and stress cycle.

a slow time t that varies from 0 to the time to the fracture time value t_* and fast time

$$\tau = \frac{t}{\mu} \quad \text{or} \quad \xi = \frac{\tau}{T_p}, 0 \le \xi \ge 1.$$

Now let us substitute the asymptotic series (2.6) into equations (2.3) – (2.4) and average the obtained equations [25, 26] by the period of stress varying. After these transformations, we get the expressions of the creep strain and the damage parameter on the time interval:

$$\left\langle c^{(0)}(\xi) \right\rangle = \int_0^1 c^0(t) d\xi = c^0(t); \quad \left\langle c^{(1)}(\xi) \right\rangle = \int_0^1 c^1(\xi) d\xi \cong 0; \tag{2.7}$$

$$\left\langle \omega^{(0)}(\xi) \right\rangle = \int_0^1 \omega^0(t) d\xi = \omega^0(t); \quad \left\langle \omega^{(1)}(\xi) \right\rangle = \int_0^1 \omega^1(\xi) d\xi \cong 0. \tag{2.8}$$

The next step is to substitute (2.7) and (2.8) into the system of equations (2.3)-(2.4). The results change the basic system to the following

$$\dot{c} = B g_n(M_k) \frac{\sigma^n}{(1-\omega)^l}; \quad \dot{\omega} = D g_m(M_k) \frac{\sigma^m}{(1-\omega)^l}; \quad \omega(0) = \omega_0, \quad \omega(t_*) = 1; \tag{2.9}$$

$$g_n(M_k) = \int_0^1 \left(1 + \sum_{k=1}^{\infty} M_k \sin(2\pi k \xi)\right)^n d\xi;$$

$$g_m(M_k) = \int_0^1 \left(1 + \sum_{k=1}^{\infty} M_k \sin(2\pi k \xi)\right)^m d\xi.$$

Here, the functions $g_n(M_k)$ and $g_m(M_k)$ reflect the influence of the cyclicity of the processes of creep and damage accumulation.

After that, let us add to the consideration the cyclic temperature varying:

$$\tilde{T} = T + T^1 = T\left(1 + \sum_{i=1}^{\infty} M_i^T \sin\left(\frac{2\pi i}{T_T} t + \beta_i^T\right)\right); \quad M_i^T = \frac{T_i^a}{T} \tag{2.10}$$

where T_i^a are the coefficients of expansion the temperature function T_1 in Fourier series. We similarly use two time scales with a small parameter $\hat{\mu} = T_T / t_*$:

$$T \cong T^{(0)}(t) + \hat{\mu} T^{(1)}(\xi). \tag{2.11}$$

Using transformations similar to those described above for creep strain (see, for example, [27, 28]), it is possible to obtain expressions for the similar influence functions $g_T(T)$ for creep and $g_T^{\omega(T)}$ for damage equation:

$$g_T(T) = B\int_0^1 \exp\left(-\frac{Q_c}{T}\left(1+\sum_{i=1}^{\infty} M_i^T \sin(2\pi i\xi)\right)^{-1}\right)d\xi; \tag{2.12}$$

$$g_T^{\omega}(T) = D\int_0^1 \exp\left(\frac{-Q_d}{T}\left(1+\sum_{i=1}^{\infty} M_i^T \sin(2\pi i\xi)\right)^{-1}\right)d\xi.$$

So, now the creep-damage laws, taking into account temperature and stress varying, can be written in the following form:

$$\dot{c} = g_n(M_k)g_T(T)\frac{\sigma^n}{(1-\omega)^l}, \quad c(0)=0; \tag{2.13}$$

$$\dot{\omega} = g_m(M_k)g_T^{\omega}(T)\frac{\sigma^m}{(1-\omega)^l}; \quad \omega(0)=\omega_0, \quad \omega(t_*)=1. \tag{2.14}$$

System (2.13) – (2.14) can be considered as a new system of governing equations for the averaged cyclic creep-damage process. Its analysis shows that when using it, there is no need to integrate over the cycle.

Next, after passing to the general case of a complex stress state with the usual use of the corresponding invariants of the stress tensor or their combination, we obtain:

$$\dot{c}_{ij} = \frac{3}{2}g_T(T)g_n(M_k^{\sigma_v})\frac{\sigma_v^{n-1}}{(1-\omega)^l}S_{ij}; \quad \dot{\omega} = g_m(M_k^{\sigma^{vd}})g_T^{\omega}(T)\frac{\sigma_{vd}^m}{(1-\omega)^l}; \tag{2.15}$$

$$\omega(0)=\omega_0, \omega(t_*)=1;$$

$$g_T(T) = B\int_0^1 \exp\left(-\frac{Q_c}{T}\left(1+\sum_{i=1}^{\infty} M_i^T \sin(2\pi i\xi)\right)^{-1}\right)d\xi;$$

$$g_T^{\omega}(T) = D\int_0^1 \exp\left(\frac{-Q_d}{T}\left(1+\sum_{i=1}^{\infty} M_i^T \sin(2\pi i\xi)\right)^{-1}\right)d\xi; \quad M_i^T = \frac{T_i^a}{T};$$

$$g_n(M_k^{\sigma_v}) = \int_0^1 \left(1+\sum_{k=1}^{\infty} M_k^{\sigma_v}\sin(2\pi k\xi)\right)^n d\xi; \quad M_k^{\sigma_v} = \frac{\sigma_v^{ak}}{\sigma_v}:$$

$$g_m(M_k^{\sigma_{vd}}) = \int_0^1 \left(1+\sum_{k=1}^{\infty} M_k^{\sigma_{vd}}\sin(2\pi k\xi)\right)^m d\xi; \quad M_k^{\sigma_{vd}} = \frac{\sigma_{vd}^{ak}}{\sigma_v}.$$

2.2.3 Cyclic Load. Overloading with Transition to Plastic Deformation

As was noted above, under forced operating modes of a gas turbine engine, in addition to the already developing creep strains, plastic strains can occur in the material of its structural elements. First, we also consider uniaxial deformation.

Let us formulate the problem. The uniaxial sample is instantly loaded in the elastic area, then deformed by creep with stress σ during time t_1. Then, for time t_2, a load is added incrementally, which realizes the stress σ_1, and its value exceeds the value of the yield limit σ_y for the given temperature. After that, the sample is also gradually unloaded to the value σ. Next, the process of loading and unloading is repeated (Fig. 2.1).

It is known [29] that an adequate description of the step load during creep can be implemented using the strain hardening theory. Let us consider it. With a stepped load from σ to σ_1, the strain rate is determined by the angle of inclination of the tangent to the strain curve with stress σ_1 at a point that can be found by parallel transfer to it along the time axis of the point from the curve constructed at stress σ. After the onset of stress σ_1, the creep strain increases according to the law corresponding to the law of its varying at the mentioned point. In the case when the stress σ_1 exceeds the yield point, we assume that the total strain also increases by stepped law by addition of plastic part. Its value can be determined by the deformation curve $(\sigma - \varepsilon)$.

Let us consider creep deformation of the rod made from high-chromium corrosion-resistant foundry heat-resistant nickel based alloy (Ni 57%, Cr 16%, Co 11%, W 5%) and heated evenly to temperature 950 C [30]. The creep curves of this material for 4 stress values for a deformation time of 1h are presented in Fig. 2.2. Note that the first two curves correspond to the deformation in which the stress values exceed the yield strength of this alloy at the given temperature σ_y = 390 MPa, the other two are obtained during the initial elastic deformation. As can be seen, the curves do not

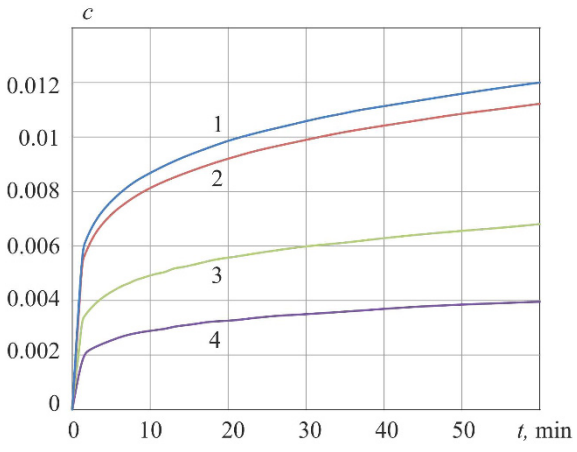

Fig. 2.2 Creep curves of heat-resistant nickel based alloy. Static loading. Stress values: 1 - 450 MPa, 2 - 420 MPa, 3 - 250 MPa, 4 - 145 MPa.

differ qualitatively. In this regard, they were processed using one dependency (2.3). It was done by use of strain hardening law. For the case of creep without damage, the following values of constants were obtained after calculations:

$$B = 5.26 \cdot 10^{-27} \text{MPa}^{-n}/\text{h}, \quad n = 5.508, \quad \alpha = 4.678.$$

Let us apply the obtained constants to Eq. (2.3) for the analysis of deformation processes with a step varying of stresses and a uniaxial stress state. To do this, we will conduct a numerical simulation of the creep process with cyclic loadings, using calculations based on strain hardening theory. A number of calculations were carried out with different input data, and below we present typical results. First, consider the loading due to Program 1 corresponding to stress varying that do not exceed the yield limit at this temperature.

2.2.3.1 Program 1

Initial value of stress σ = 250 MPa, the greater value σ_1 = 350 MPa, t_0=0.166 h (10 min), t_1 = 0.083 h (5 min), t_2 = 0.25 h. Loading time is equal to 1 h. The results are presented in Fig. 2.3, where the dependence of the total strain ε ($\varepsilon = \varepsilon^{elast} + c$) on time is given. Here, curve 1 and 3 correspond to the static load at σ = 350 MPa, curve 3 – at σ = 250 MPa. Curve 2 is built for data from cyclic loading according to program 1. As can be seen from the figure, the curve for cyclic loading is similar to

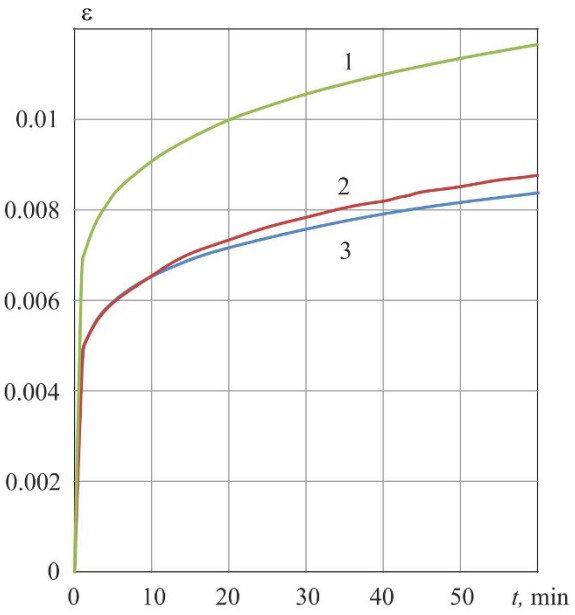

Fig. 2.3 Creep curves of heat-resistant nickel based alloy. Static (curves 1 - 350 MPa and 3 - 250 MPa) and cyclic (curve 2) loading.

the curves for static loading, therefore, it is possible to use the ratio of type (2.13) to describe the averaged process.

2.2.3.2 Program 2

Now consider the load according to program 2, in which the load in the plastic zone is cyclically added to the creep caused by the stress, which exceeds the yield strength. We analyse the case of deformation with hardening of the material in each cycle of additional loading, when the yield stress changes due to hardening process, as shown in Fig. 2.4.

Initial value of stress σ = 370 MPa, the greater value σ_1 = 420 MPa, t_0 = 0.25 h, t_1 = 0.083 h, t_2 = 0.083 h. Loading time is equal to 1 h. The results are shown in Fig. 2.5. As can be seen from the comparison of the location of curves 2 in Figs. 2.3 and 2.5, they are qualitatively different, which is due to the instantaneous plastic additional loading in the cycle of program 2. With a rather small difference between the stress values σ and σ_1 in 50 MPa, we observe jumps in deformation during additional loading. During unloading, there is an elastic reduction, but the plastic strain accumulated during the cycle remains and is added to the full value. It is also possible to see that with each cycle as the yield strength increases, the amount

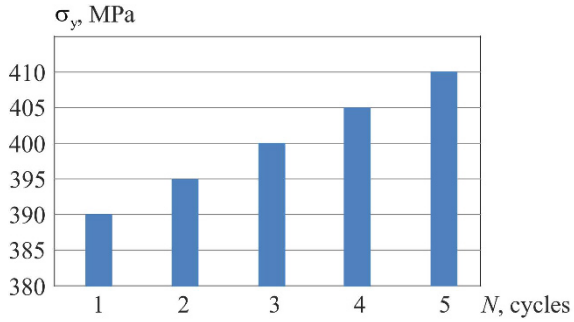

Fig. 2.4 Dependence of the yield limit on the number of the loading cycle.

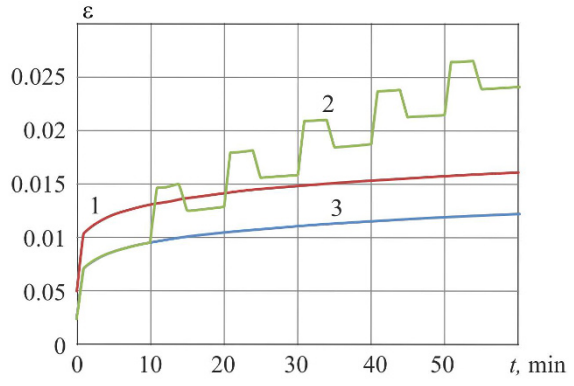

Fig. 2.5 Creep curves of heat-resistant nickel based alloy. Static (curves 1 - 420 MPa, and 3 - 370 MPa) and cyclic cyclic step loading according to program 2 (curve 2).

of reduction in total strain also decreases. This means that when loading has a lot of cycles, the shape of the strain curve will approach a smoother one. A similar conclusion is confirmed by the shape of the strain curve with 10 similar cycles of program 2, which is presented in Fig. 2.6. A loading time of 2 h was set.

From the analysis of the curve in Fig. 2.6, built according to program 2 of the step loading, it can be seen that when the current value reaches the yield strength value of the acted stress σ_1 = 420 MPa, the deformation begins to proceed similarly to the process with initially elastic stresses (as according to program 1). Such loading processes are similar to ratcheting processes [31], but with continued growth of creep strains.

The method of obtaining the averaged equations discussed in the previous section cannot be used directly to obtain the averaged equation in the case when there is an overloading in the cycle, which leads to the occurrence of plastic strains with material hardening. This is due to the different nature of curves for the cyclic creep with plastic strains creep under static loading. In this regard, an approach is proposed that allows obtaining an approximate form of such an averaged equation, for its use in numerical modeling of structural elements of turbomachines.

Let us assume that due to experiments or numerical modeling using strain hardening law (it is this that makes it possible to calculate the case of additional loading [29]) a set of uniaxial creep curves under purely static loading and a corresponding set of curves for the case of cyclic overloads is obtained (Fig. 2.7). The set should consist of as many calculated curves as possible (three are shown in the figure to better understand the appropriate arrangement). As can be seen after analyzing the curves of the Fig. 2.7, the cyclic overload curves in the case under consideration with stress values from 390 to 420 MPa are of the same type. They are characterized by higher values of strains in the cycle at higher values of overload stresses. After the overload is completed, the strains follow the same segments of the curves corresponding to the main static load. This means that the function of irreversible cyclic deformation does not depend on the value of the overload stresses, but only on the stress of basic loading.

Next, for each curve of cyclic creep with overloads, using approximation procedures, we obtain averaged curves, i.e., curves that correspond exactly to the irreversible

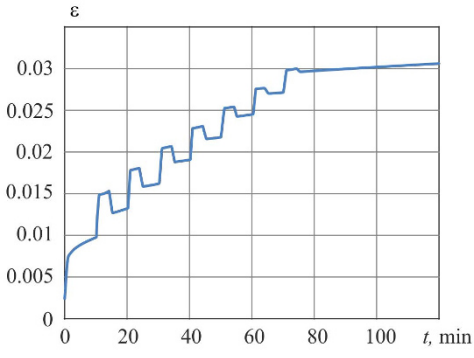

Fig. 2.6 Cyclic creep curve of heat-resistant nickel based alloy (program 2).

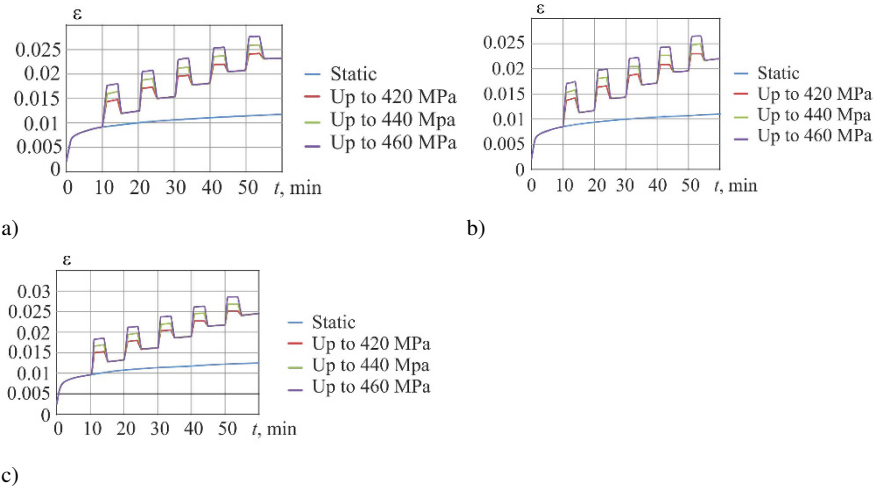

Fig. 2.7: Creep curves of heat-resistant nickel based alloy for static stresses (a) 330 MPa, b) 350 MPa, c) 370 MPa) and cyclic overloading up to 420, 440 and 460 MPa.

strain accumulated in the sample. This is shown in Fig. 2.8, where the cyclic creep curve with the overload amplitude σ_1 (curve 1), the averaged curve 2 and the curve under static loading (3) are presented for one set of applied stress values. Points used for approximation are marked with circles.

Using classical methods of processing the static creep curves, we find the values of the constants B, n, α , included in the equation for the static creep strain rate function:

$$\dot{c} = Bc^{-\alpha}\sigma^n \tag{2.16}$$

Further, by integrating Eq. (2.16), we obtain an expression for the dependence of creep strains on time:

$$c_j = b\sigma_j^r t^a, \quad j = 1 \ldots N, \tag{2.17}$$

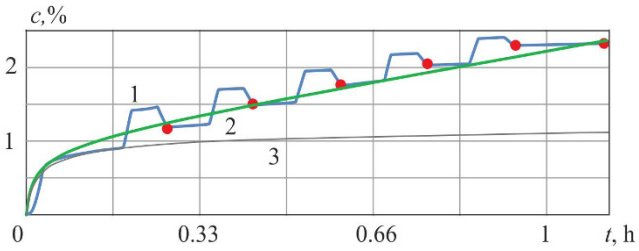

Fig. 2.8: Schematic presentation of the cyclic creep curve (1), averaged curve (2) and static creep curve (3).

where B, r, a are the constants, N is the number of curves obtained. According to the procedure described above for obtaining averaged curves of irreversible strain (curve like curve 2 in Fig. 2.8), we obtain approximation dependencies for these functions $f_j(t;\sigma_j), j = 1 \ldots N$. Than it is possible to determine the influence function in the form of the additional coefficient $k_j(t;\sigma_j)$, multiplied by which the value of the function of static creep strains (curve 3 in Fig. 2.8) the demanded value on the averaged curve 2 will be obtained:

$$k_j(t;\sigma_j) = \frac{f_j(t;\sigma_j)}{b\sigma_j^r t^a}, \quad j = 1 \ldots N, \tag{2.18}$$

Next, using the values of the obtained functions $k_j(t;\sigma_j)$ at N points on the plane (t,σ) for each of the set of points (t_i,σ_j) $(i = 1 \ldots M)$ we obtain the values of the function $K(t_i,\sigma_j)$, which reflects the effect of cyclic loading on creep. With the help of approximation procedures in the two-dimensional domain, we obtain the expression of the function $K(t,\sigma)$ for the all possible values of times and stresses. It is already possible to include it in calculations for cyclic loading. For the function of cyclic creep strains, we obtain

$$c = K(\sigma,t)b\sigma^r t^a, \tag{2.19}$$

or for the cyclic creep strain rate function

$$\dot{c} = \dot{K}(\sigma,t)b\sigma^r t^a + aK(\sigma,t)b\sigma^r t^{a-1} \tag{2.20}$$

For the case of a complex stress state, we get:

$$\dot{c}_{ij} = \frac{3}{2} b\sigma_v^{r-1} \left(\dot{K}(\sigma_v,t)t^a + aK(\sigma_v,t)t^{a-1}\right) S_{ij} \tag{2.21}$$

The analysis of expression (2.21) shows that it provides the possibility of simulating creep processes with overload stresses in the cycle exceeding the yield limit, using only the formulation of the creep problem under static loading, but with an governing equation of the type (2.21).

To illustrate the method of obtaining an equation of type (2.21), which allows calculations for a wide range of stresses of the main loading process σ, let us continue the analysis of the deformation of considered alloy at a temperature of 950°C. As an example, consider curves 2 and 3 of Fig. 2.5. The value of the static stress $\sigma = 370$ MPa. We will use curve 2 to obtain a new curve that will correspond to curve 2 in Fig. 2.8, which is an averaged curve that collectively describes the development of irreversible strains during creep with overloads. Such a curve is constructed - it is curve 1 in Fig. 2.9. The points show the values taken from curve 2 of Fig. 2.5 at moments of partial unloading.

Next, it was necessary to construct a function that would approximate above mentioned curve 1 from Fig. 2.9. After a number of mathematical experiments, it was found that the hyperbolic function best satisfies the conditions of approaching the experiment in the first cycles and reaching the asymptote at larger time values. It

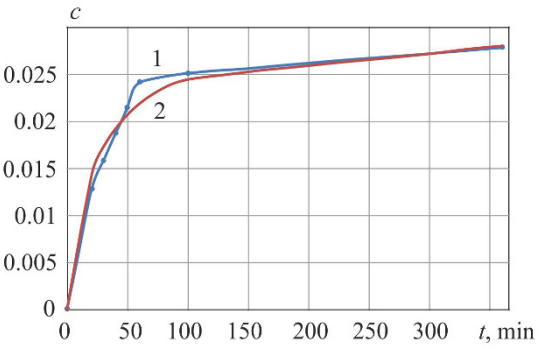

Fig. 2.9 The averaged deformation curve during creep with overloads (1) and the approximated curve (2).

was accepted in the following form:

$$c = \frac{t}{b_0 + b_1 t} \tag{2.22}$$

The values of constants are included in (2.22): $b_0 = 742.61$ min, $b_1 = 33.82$. The graph of this function is represented by the curve 2 in Fig. 2.9. As can be seen from the comparison of the values presented on curves 1 and 2 of this figure, the worst difference that occurs in the area after the fourth unloading does not exceed 10%. On other sections, and most importantly, on larger time values, the differences are 2-3%. This is satisfactory for calculations.

Next, let us consider the deriving of function $K(t, \sigma)$. For this, it was necessary to carry out similar actions with the curves obtained for other stress values like presented above for the case of $\sigma = 370$ MPa. The stress values were taken in the range of 295-370 MPa with a step of 15 MPa. For each of these creep curves with overloads, an approximation algorithm was performed and constants to Eq. (2.22) were found. They were close enough to presented in (2.22). After that, it was possible to determine the values of the coefficients $k_j(t; \sigma_j)$ for expression (2.18). The calculations were carried out for the above stress values and time of 100 min with a step of 20 min. Thus, for each of the 36 points, the coefficients $k_j(t; \sigma_j)$ were found. They are represented by the surface $K(t, \sigma)$ in Fig. 2.10.

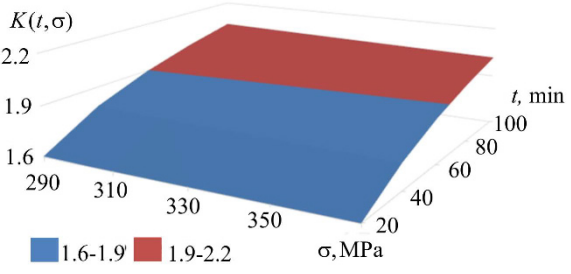

Fig. 2.10 Dependence of the function $K(t, \sigma)$, reflects the influence of the cyclic overloads on creep rates, from the stress values of the main process and time.

After that, the obtained digital values function $K(t,\sigma)$ of two coordinates in the plane, time and stresses, were used for the numerical determination using the approximation algorithm of the function of two variables. The analytical expression of the function $K(t,\sigma)$ was obtained as follows:

$$K(t,\sigma) = V_0 \sigma^{v_1} t^{v_2} \tag{2.23}$$

where numerical constants included have the following values:

$$V_0 \;=\; 0.785\text{MPa}^{-v_1}\text{h}^{-v2}, \quad v_1 = -0.32, \quad v_2 = 0.15.$$

To use this function when calculating a complex stress state, it is necessary to make a transition to equivalent stresses and strains due to (2.21) according to relations (2.23) as well as to obtain the expression of creep strain rate. We obtain:

$$\dot{c}_{ij} = \frac{3}{2} b V_0 \left(a + v_2\right) \sigma_v^{r-1+v_1} t^{v_2+a-1} S_{ij} \tag{2.24}$$

2.3 Problem Statement

Let us consider the general mathematical formulation of the boundary initial value problem of the creep of deformed solids for the volume V with isotropic properties in the Cartesian coordinate system $x_i (i = 1,2,3)$. It us supposed, that non-varied in time displacement values are known in the part of solid's surface S_1 $u_{i|S_1} = \bar{u}_i$. Another surface part S_2 is loaded by traction p with constant in time $p_i^0(x)$ and cyclically varied in time $\Phi_i(x,t)$ components:

$$p_i(x,t) = p_i^0(x) + \Phi_i(x,t), \;\; x \in S_2 \tag{2.25}$$

where

$$\Phi_i(x,t) = p_i^a(x)\Phi(t) = p_i^a(x) \sum_{k=1}^{\infty} A_k \sin\left(\Omega_k t + \beta_k^p\right) \tag{2.26}$$

are the periodical expansions with period T_p;

$$p_i^a(x), \;\; A_k = \sqrt{a_k^2 + b_k^2}, \;\; \Omega_k = 2\pi k / T_p, \;\; \beta_k^p = \arctan\left(a_k / b_k\right)$$

are known values.

The solid V is an inhomogeneous temperature field, which is set on the surface S by the sum of the constant T and periodically varying T_1 components:

$$\tilde{T}(x,t) = T(x) + T^1(x,t), \;\; x \in S, \tag{2.27}$$

where

$$T^1(x,t) = T^a(x)\theta(t) = T^a(x)\sum_{k=1}^{\infty} A_k^T \sin\left(\Omega_k^T t + \beta_k^T\right), \tag{2.28}$$

are the periodical expansions with period T_T;

$$T^a(x),\ \ A_k^T = \sqrt{\left(a_k^T\right)^2 + \left(b_k^T\right)^2},\ \ \Omega_k^T = 2\pi k/T_T,\ \ \beta_k^T = \arctan\left(a_k^T/b_k^T\right)$$

are known values.

Due to Lagrange approach we consider the small strains and displacements that usually occur in the structural elements of power engineering. The following notations are used: $\mathbf{u}$ for displacement vector with components $u_i(x,t)$; $\boldsymbol{\sigma}$, $\boldsymbol{\varepsilon}$ are the stress and strain tensors with components $\sigma_{ij} = \sigma_{ji}(x,t)$ and $\varepsilon_{ij} = \varepsilon_{ji}(x,t)$. Both of them are functions of co-ordinates x_i $(i = 1, 2, 3)$ and time t. Let us assume that at any time the strain tensor is the sum of elastic and temperature strain tensors, tensors of irreversible plasticity and creep strains:

$$\varepsilon_{ij} = \varepsilon_{ij}^e + \varepsilon_{ij}^T + \varepsilon_{ij}^p + c_{ij}, \tag{2.29}$$

where $\boldsymbol{\varepsilon^e}, \boldsymbol{\varepsilon^T}$ are the elastic and thermal strain tensors with components $\varepsilon_{ij}^e(x)$, $\varepsilon_{ij}^T(x)$; $\boldsymbol{\varepsilon^p}$ is plastic strain tensor with components $\varepsilon_{ij}^p = \varepsilon_{ij}^p(x)$; $\mathbf{c}$ is creep strain tensor with components $c_{ij} = c_{ji}(x,t)$, $c_{ij}(x,0) = 0$, $(i,j = 1,2,3)$.

For thermal strains, let's limit ourselves to the generalized law of thermoelasticity of homogeneous isotropic solids [24], known as the Duhamel-Neumann law, so that at any time the relationship between stresses, strains and temperature is written as follows:

$$\sigma_{ij} = \lambda\varepsilon_0\delta_{ij} + 2G(\varepsilon_{ij} - \varepsilon_{ij}^p - c_{ij}) - (3\lambda + 2G)\varepsilon_{ij}^T; \tag{2.30}$$

$$\varepsilon_0 = \varepsilon_{km}\delta_{km};\ \ \lambda = \frac{\nu E}{(1+\nu)(1-2\nu)};\ \ G = \frac{E}{2(1+\nu)};\ \ \varepsilon_{ij}^T = \alpha_{Te}\tilde{T}\delta_{ij}$$

where λ, G are Lamé parameters; α_{Te}, δ_{ij} are coefficient of thermal expansion and Kronecker delta.

As in [25–27], we present the basic system of equations for determining the stress-strain state of the solid during creep under the conditions of a known temperature field $\tilde{T}(x,t)$

$$\sigma_{ij,j} = \rho\ddot{u}_i;\ \ x_i \in V;\ \ \sigma_{ij}n_j = p_i^0(x) + \Phi_i(x,\ t),\ \ x_i \in S_2; \tag{2.31}$$

$$\varepsilon_{ij} = \frac{1}{2}\left(u_{i,j} + u_{j,i}\right), x_i \in V;\ \ u_i|_{S_1} = \bar{u}_i,\ \ x_i \in S_1;$$

$$\sigma_{ij} = \lambda\varepsilon_0\delta_{ij} + 2G(\varepsilon_{ij} - \varepsilon_{ij}^p - c_{ij}) - (3\lambda + 2G)\alpha_{Te}\tilde{T}\delta_{ij}$$

where, in addition to the previously defined notations, $\mathbf{n}$ is a unit vector with components n_i, $i = 1,2,3$ of the external normal to the solid's surface.

The system of differential equations (2.31), which should be specified by adding to it the constitutive equations of the material (2.15), will describe the general mathe-

matical formulation of boundary- initial value creep-damage problem at periodically varying temperatures and stresses. To apply the constitutive equations, let us transform the system of differential equations (2.30) using the method of two time scales and averaging over the period of the cyclic varying the components of temperature and stress.

Let us assume that the time of the creep process until the completion of the hidden damage is much longer than the periods of the cyclic components of stress and temperature $t_* \gg \max(T_p, T_T)$, and limit ourselves to the first approximation of the asymptotic expansions for the components $\mathbf{u}$, $\boldsymbol{\varepsilon}$ and $\boldsymbol{\sigma}$ with a small parameter $\mu = \min[(t_*/T_p)^{-1}, (t_*/T_T)^{-1}]$, $\mu \ll 1$:

$$u_i \cong u_i^{(0)}(x, t) + \mu\, u_i^{(1)}(x, \xi), \quad \varepsilon \cong \varepsilon^{(0)}(x, t) + \mu\, \varepsilon^{(1)}(x, \xi);$$

$$\varepsilon_{ij}^T \cong \varepsilon_{ij}^{T(0)}(x, t) + \mu\, \varepsilon_{ij}^{T(1)}(x, \xi), \quad \varepsilon_{ij}^p \cong \varepsilon_{ij}^{p(0)}(x, t) + \mu\, \varepsilon_{ij}^{p(1)}(x, \xi); \tag{2.32}$$

$$\sigma_{ij} \cong \sigma_{ij}^{(0)}(x,t) + \mu\sigma_{ij}^{(1)}(x,\xi), \quad c_{ij} \cong c_{ij}^{(0)}(x,t) + \mu c_{ij}^{(1)}(x,\xi)$$

where x, t and ξ are formally independent variables. Then, after performing the transformations that can be found in [25, 26], we obtain two systems of equations - the main (2.33) and auxiliary (2.34).

System (2.33) describes the motion of a system of material points during irreversible deformation on a slow time scale:

$$\sigma_{ij,j} = 0, \quad x_i \in V; \quad \sigma_{ij} n_j = p_i^0, \quad x_i \in S_2; \tag{2.33}$$

$$\varepsilon_{ij} = (u_{i,j} + u_{j,i})/2, \quad x_i \in V; \quad u_i|_{S_1} = \bar{u}_i, \quad x_i \in S_1;$$

$$\sigma_{ij} = \lambda\varepsilon_0\delta_{ij} + 2G(\varepsilon_{ij} - \varepsilon_{ij}^p - c_{ij}) - (3\lambda + 2G)\alpha_{Te} T\delta_{ij}.$$

Here, and in following text, the superscript "0", that describe the creep processes of heterogeneously heated solids that occur on a slow time scale, is omitted in the functions.

The system of equations (2.33) should be supplemented with the creep-damage constitutive equations (2.15). This system describes the general mathematical formulation of the boundary initial value creep-damage problem at periodically varying temperatures and stresses.

To specify the system of equations (2.33), which must be applied with use of constitutive equations (2.15), it is necessary to define the stress fields σ_{ij}^{ak}, $k = 1, 2, \ldots$. as well as temperature fields T_i^a, $i = 1, 2, \ldots$, which describe the periodically varying processes of the stress-strain state and temperature over time ξ, $0 \le \xi \le 1$. Auxiliary systems of equations are intended for this purpose. A system of equations is obtained for time scale ($0 \le \xi \le 1$) [26, 27]:

$$\sigma_{ij,j}^{(1)} = \rho\mu^{-3} u_{i,\xi\xi}^{(1)}; \quad \sigma_{ij}^{(1)} n_j = \mu^{-1}\Phi_i, \quad x_i \in S_2; \tag{2.34}$$

$$\varepsilon_{ij}^{(1)} = (u_{i,j}^{(1)} + u_{j,i}^{(1)})/2, \quad x_i \in V; \quad u_i^{(1)}\Big|_{S_1} = 0, \quad x_i \in S_1;$$

$$\sigma_{ij}^{(1)} = \lambda\varepsilon_0^{(1)}\delta_{ij} + 2G\varepsilon_{ij}^{(1)} - (3\lambda + 2G)\alpha_{Te}T^1 - \sigma_{ij}^{(1)p}.$$

The system of equations (2.34) corresponds to the equations of thermoelasticity (thermoplasticity in the case of the presence of plastic overloads in the cycle) of the solid at given periodically varying loading with frequencies which is significantly lower from lower solid's natural frequency Ω_0: $(\Omega^p = 2\pi/T_p,\ \ \Omega^T = 2\pi/T_T) \ll \Omega_0$. The traction and temperature functions are specified on the corresponding parts of the solid's surface:

$$\Phi_i(x,\xi) = p_i^a(x)\Phi(\xi) = p_i^a(x)\sum_{k=1}^{\infty}\Phi_k(\xi),\ \ \Phi_k(\xi) = A_k\sin\left(\mu\Omega_k\xi + \beta_k^p\right), \quad (2.35)$$

$$T^1(x,\xi) = T^a(x)\theta(\xi) = T^a(x)\sum_{k=1}\theta_k(\xi),\ \theta_k(\xi) = A_k^T\sin\left(\mu\Omega_k^T\xi + \beta_k^T\right).$$

This allows us to consider system (2.34) as corresponding to the non-stationary deformation of the body under the action of harmonically varying pressure on the surface S_2 $p_{ik}^{(1)} = p_i^a(x)\varphi_k(\xi)$, where $\varphi_k(\xi) = \Phi_k(\xi)/\mu$, $\varphi_{k,\xi\xi} = -\mu^2\Omega_k^2\varphi_k(\xi)$ (as a harmonic function). If the periods of traction and temperature are assumed to coincide, then, as is known, in (2.34) it is possible to separate the variables by coordinates and time

$$\sigma_{ij}^{(1)} = \sum_k \sigma_{ij}^{ak}(x)\varphi_k(\xi), \quad (2.36)$$

$$u_i^{(1)} = \sum_{k=1} u_i^{ak}(x)\varphi_k(\xi),$$

$$T^1 = \sum_{k=1} T^{ak}(x)\varphi_k(\xi).$$

Boundary value problems for amplitude values of unknowns periodically varying on a fast time scale will have the following form $(k = 1, 2, \ldots)$:

$$\sigma_{ij,j}^{ak} = -{\Omega_k}^2\mu^{-1}\rho u_i^{ak},\ \ \sigma_{ij}^{ak}n_j = p_i^a(x)A_k,\ \ x \in S_2; \quad (2.37)$$

$$\varepsilon_{ij}^{ak} = 1/2\left(u_{i,j}^{ak} + u_{j,i}^{ak}\right);\ \ x \in V;\ \ u_i^{ak} = 0,\ \ x \in S_1;$$

$$\sigma_{ij}^{ak} = \lambda\varepsilon_0^{ak}\delta_{ij} + 2G\varepsilon_{ij}^{ak} - (3\lambda + 2G)\alpha_{Te}T^a(x)A_k^T - \sigma_{ij}^{pak}.$$

Inertial components in the first equations of system (2.37) are formally preserved when deriving the equations, meanwhile, they can be neglected in calculations, under the conditions of considering the processes with far from resonant frequencies $\Omega^p = \Omega^T \ll \Omega_0$. Under this assumption, systems (2.37) can be considered as a static problem of thermo-elasticity (thermo-plasticity).

Amplitude values of unknowns periodically varying on a fast time scale are calculated after solving the problem of non-stationary thermal conductivity for the heating-cooling cycle and determining the value of the function $T^{(1)}$. This makes it possible to solve systems of Eqs. (2.37).

According to the algorithm proposed above, after solving the initial-boundary value problem (2.33), the stress-strain state of the solid's creep-damage process with cyclic varying of temperature and external force fields is determined. Its integration is carried out until the finish of hidden damage accumulation or until the time for the analysis of the deformation process, which is specified by the problem conditions.

2.4 Comparison Between Data of Direct Approach and Use of Averaged Function *K*

Next, let us proceed to the analysis of the results of solving the problem of creep under intermittent overloads, which lead to the occurrence of plastic deformation. In this case, the traction p varyings according to the time law, which is similar to the presented in Fig. 2.1.

Let us consider the creep of a long plate (beam) subjected to bending in its plane by a traction part p_b=1 MPa and tensed by an another traction part p_e, which has a constant value of 25 MPa up to the middle of the plate, and then increases linearly to 75 MPa. Such a load can be considered as simulating the behavior of a turbomachine blade, which is loaded by surface pressure from the working body (bending) and tensed by centrifugal forces. The left edge of the plate is rigidly fixed.

Plate dimensions: length 100 mm, width 12 mm, thickness 1 mm. The plate is periodically loaded with both types of load in such a way that plastic strains occur in a certain part of it. At the same time, p_b reaches the value p_{bo}=1.45 and p_{eo} = $1.45p_e$. It has a constant value of 36.25 MPa up to the middle of the plate, and then increases linearly to 109 MPa. The material of the plate is the above considered nickel based alloy at a temperature of 950°C. The considered conditions correspond to a two-dimensional plane stress state.

For the direct numerical modeling of considered cyclic creep process, it was necessary to solve a number of boundary and initial-boundary problems, namely:

1. creep under tensile load p_b and p_e during t_0 =0.25 h;
2. instantaneous elastic-plastic loading with load $p_{bo} + p_{eo}$;
3. creep under load $p_{bo} + p_{eo}$ during t_1 =0.25 h to 0.5 h;
4. unloading to $p_b + p_e$;
5. creep under load $p_b + p_e$ during t_2 =0.25 h to 0.75 h;
6. instantaneous elastic-plastic loading to load $p_{bo} + p_{eo}$;
7. creep under load $p_{bo} + p_{eo}$ during t_1 =0.25 h to 1 h.

After studies of the convergence of the solutions, a FE mesh with 600 elements and 357 nodes was involved in the calculations. Computer simulation was carried out and the results of sequential data calculation of these 7 problems were obtained. The results in the form of the final distribution of von Mises strains in the beam are shown in (Fig. 2.11a). The areas of the beam where irreversible plastic strains take place are marked with ovals. As you can see, they occupy a very limited area near the fixed side.

Fig. 2.11: Distributions of von Mises equivalent strain in a beam area. a) - direct solution of 7 creep and plastic problems; b) – calculations with use of Eq. (2.24).

Next, the same elastic-plastic-creep behavior of the beam under consideration was modeled using the obtained Eq. (2.24), which uses the influence function $K(\sigma_{vM}, t)$ and reflects the effect of cyclic overloads. The result in the form of a similar distribution of von Mises strains in the beam is shown in (Fig. 2.11b). Comparing the distributions obtained by direct integration (Fig. 2.11a) and by using the influence function (Fig. 2.11b), we conclude that calculations based on the equivalent rate of irreversible strains qualitatively and quantitatively correctly determine the location and level of maximum strains. In the rest beam area, the deviations between the distributions are also minimal. Somewhat larger strains occur around the zones near the fixed side, which are about 0.5%. Such a deviation can be considered as satisfactory, taking into account the fact that when determining long-term strength based on calculations of accumulated damage, the area of maximum stresses and strains is decisive. The obtained conclusion regarding the satisfactory degree of accuracy when solving problems with overloading in the cycle, which leads to the occurrence of plastic strains, allows us to use the proposed approach for the modeling the deformation of more complex structural elements.

2.5 Numerical Simulation of the Cyclic Creep-damage in DWTC System Model

As noted in the literature review, cooled systems and blades (common name Double-wall transpiration cooling system - DWTC system) are now widely used in practice -

both in gas turbines and in turbines [6, 8]. Real blades are three-dimensional objects with a rather complex geometric shape, with a large number of different cooling channels. Correct numerical simulation of such objects by FEM using requires the meshes with a very large number of finite elements (of the order of 10^6) as well as large amounts of computer resources. In the presence of such data volumes, their processing in order to identify qualitative patterns of deformation and damage is not a simple task, and errors in solving physically nonlinear problems that accumulate when using models with a large number of elements can lead to incorrect conclusions.

In this regard, the papers have been published, in which the behavior of DWTC systems is simulated using simpler models (for example, rod models in [12]). Using analytical and approximate methods for such a model, it was possible to obtain a number of qualitative regularities of the behavior of the systems under consideration. But the important factors of non-homogeneous temperature and stress distributions, stress redistribution during physically nonlinear deformation remained unconsidered.

However, it is proposed to develop this approach in the direction of, on the one hand, the complication of the model, so that it reflects the main features inherent in a complex stress state, and on the other hand, so that the correct numerical simulation can take place in an acceptable time frame (the calculation time of one variant should not exceed 20-30 min). Also, this model should be built based on those approaches that are used in the engineering analysis of structural elements, namely the FEM approaches. Therefore, in this paper, the construction of a simplified two-dimensional model of a cooled turbine blade is proposed. At the same time, the main components of the thermal load inherent in the deformation of such blades will be taken into account: non-uniform temperature distribution due to the effect of the cooling, non-uniform pressure on the blade and the contribution of centrifugal forces. There remains the possibility of expanding the field of research, for example, due to the addition of new cooling channels to the model, the possibility of making a blade from different materials, etc.

2.5.1 Description of the Calculation Model

A model of a structural element with a plane cross-section, which has two walls and a bridge between them, simulating the effect of a blade's shelf (Fig. 2.12), is involved in the simulation. The following dimensions were set: total height $h = 0.3$ m, shelf length $L = 0.09$ m, shelf height $h_1 = 0.06$ m, blade height $h_2 = 0.235$ m, blade wall thickness $h_w = 0.024$ m, cooling channel width $a = 0.018$ m. The lower surface is rigidly fixed. The load consist of pressure from the gas flow, action of centrifugal loads.

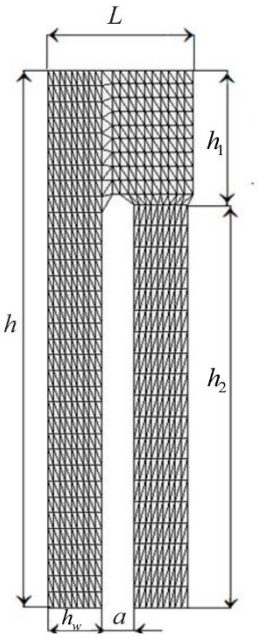

Fig. 2.12 FE scheme and main dimensions of the blade model.

2.5.2 *Determination of the Temperature and Stress Field in the Blade*

In this modelling cycle, we will consider the steady-state temperature field that is created in the blade during its steady-state cooling. For calculations, we use the developed research program *FEM Temperature 2d*. Let us use the boundary conditions of the 1^{st} kind and set the temperature distribution along the model's boundaries.

Let us consider several boundary conditions of the same type, which differ by the level of blade heating. On the left edge (see Fig. 2.12) the temperature T_l is set, inside the model, on the edges of the cooling channel T_{in}, on the right side is the temperature that varies from T_l on the shelf to T_{rmin} on the blade.

A special preprocessor program for generating FE meshes has been developed for numerical modelling. An example of its operation for a model with 18 FE in wall thickness, a total of 1170 elements, is shown in Fig. 2.12. The results of solving the stationary thermal conductivity problem in the form of temperature distribution in finite elements are shown in the figures in the corresponding subsections.

Let us discuss the problem of the refinement of stress state. In the case of solving the problem of thermo-elasticity at the initial stage of integration, the considered calculation scheme has a defect associated with the presence of large unphysical values of stresses in the boundary. In the real design, the blade is further continued by the root, which is in contact with the locking joint. To clarify the stress-strain state in

the proposed model, a real complex analysis of the stress-strain state of such a blade was performed. The used calculation scheme is presented in Fig. 2.13.

The results of the thermoelastic analysis of the stress-strain state for the three-dimensional model of the blade are presented in Fig. 2.14 a) (temperature distribution) and 2.14 b) (distribution of von Mises equivalent stress). From the analysis of the stress state calculation, it can be seen that there are increased stress values in the area of the transition from the blade to the root.

In this regard, for the creep-damage simulation in the blade model using the calculation scheme presented in Fig. 2.12, stress values in a von Mises stress range from 360 MPa to 260 MPa are considered in the area of the model's fixation.

2.5.3 *Creep Calculations for a Two-dimensional Model of a Blade Made of Nickel Based Alloy*

Let us consider the results of the cycle of calculations of the stress-strain state accumulation in the blade model given in Fig. 2.12. Blade material is high-chromium corrosion-resistant foundry heat-resistant nickel based alloy (Ni 57%, Cr 16%, Co 11%, W 5%) [30]. Temperature range: 950-850°C. $T_1 = 950°C$, $T_{in} = 850°C$, $T_{rmin} = 900°C$. The distribution of the temperature field along the cross section of the model, which is consistent with that obtained for the 3D model (2.14) a), is given in Fig. 2.15.

Let us consider the case of loading the lateral face of the blade with pressure from the gas flow, which varies according to the functional dependence on the height of the blade as a set of linear sections. The graph of this dependence is shown in Fig. 2.16 a).

The action of centrifugal loads with an intensity of 8 MPa is given. Temperature stresses are taken into account. The results of the calculations in the form of distributions of the von Mises stress fields along the cross section of the model are given in Fig. 2.16. Figure 2.16 b) contains data obtained for the case of pressure acting

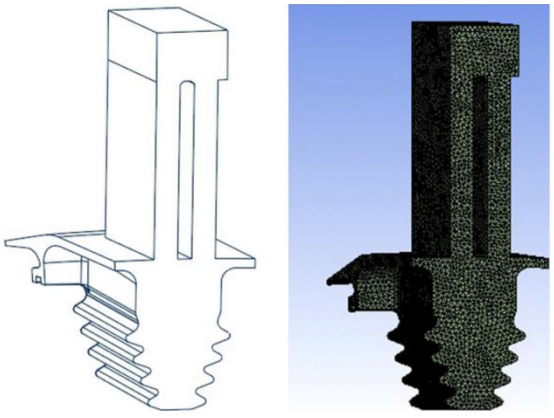

Fig. 2.13 A sketch of a simplified blade model and its FE mesh.

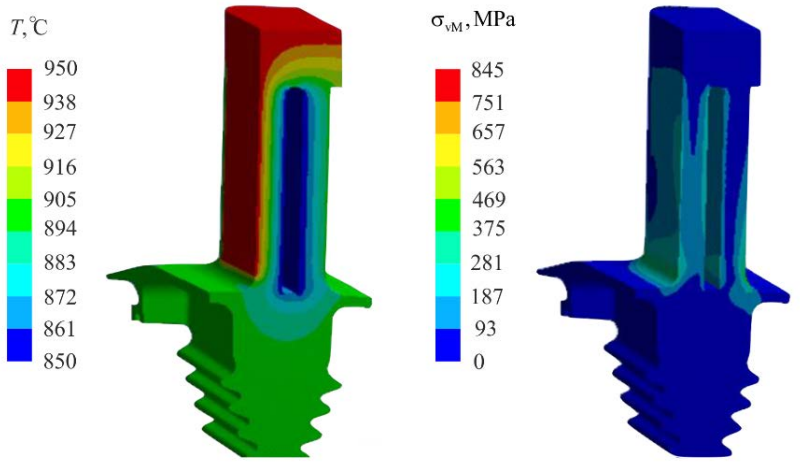

Fig. 2.14: Calculation results in a three-dimensional statement: a) – temperature distribution; b) – distribution of von Mises equivalent stresses. $t = 0$ h.

Fig. 2.15 Temperature distribution along the cross-section of the FE model, blade made from nickel based alloy (Ni 57%, Cr 16%, Co 11%, W 5%).

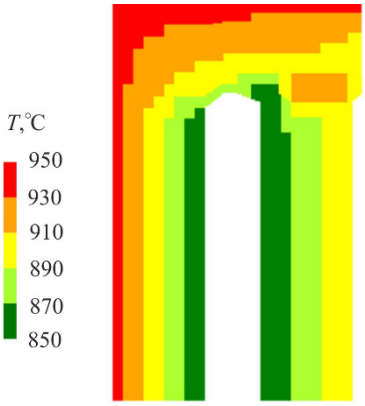

according to the law given in Fig. 2.16 a), as well as Fig. 2.16 b) for the case of constant pressure with a value of 13 MPa, which corresponds to the average value of pressure when using the law presented in Fig. 2.16 a). Comparing these distributions, we come to a conclusion about the practical closeness of the results. In this regard, further calculations were performed for the case of constant pressure. Note that the stress values obtained in the thermoelastic calculation do not exceed the yield strength for the given temperature of 950°C, $\sigma_y = 390$ MPa.

First, let us consider the results of numerical modeling of the blade behavior under the action of only static loads. The constitutive equations (2.3), (2.4) are applied. Let

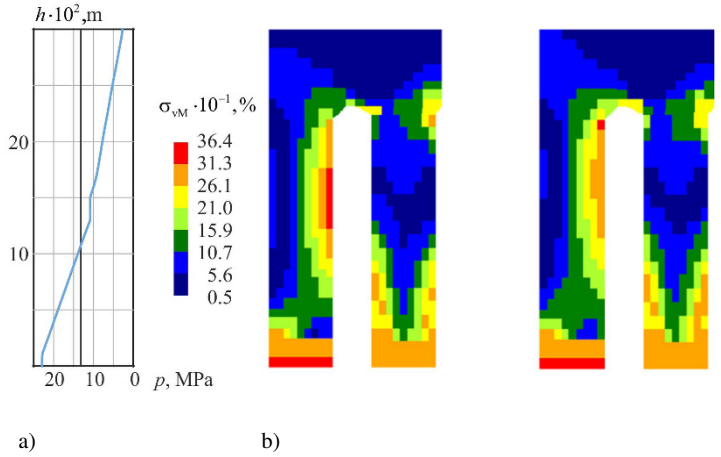

Fig. 2.16: Distributions of pressure (a) and of von Mises stress (b). Blade made from nickel based alloy (Ni 57%, Cr 16%, Co 11%, W 5%). Static loading. $t = 0$ h..

us present in addition to described creep constants of considered alloy the values of constants are included in damage evolution equation (2.4): $D = 1.1810^{-17}\text{MPa}^{-m}/\text{h}$, $m = l = 5.69$. The result of calculations show that the time of hidden damage accumulation is equal to 24.16 h. The obtained distributions of von Mises strains (a) and damage parameter (b) for this time value are presented in Fig. 2.17.

It can be seen from the obtained data that the largest strains are in the left side of a blade not so far to the transition zone to the blade root. The maximum value reaches 1.7%. Also, the similar strain values occur in the area of stress concentration near

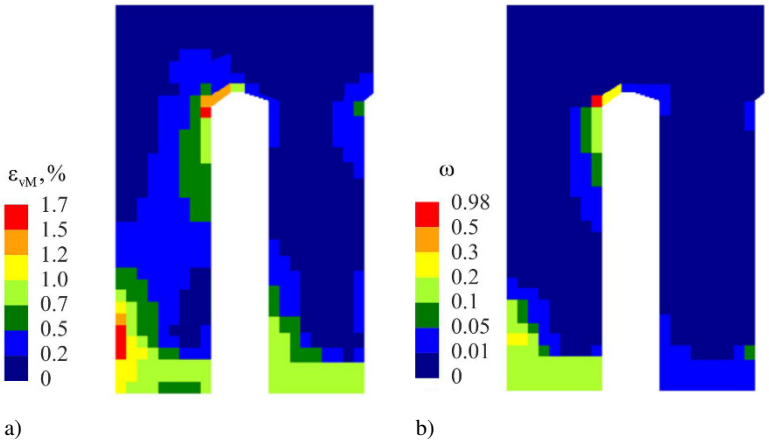

Fig. 2.17: Distribution of the von Mises strain (a) and damage parameter (b), blade made from nickel based alloy (Ni 57%, Cr 16%, Co 11%, W 5%). Model 1, static loading. t= 24.16 h.

the blade shelf. The fracture occurs in this place, but traditional type of the fracture in the blade fixed area is possible due to fairly high values of damage parameter (0.2-0.3) here. This area is characterized by joint action of temperature stresses and gas pressure.

Further let us present the data of calculation with considering cyclic overloading of blade with plastic deformation through a cycle. The influence function $K(\sigma_v, t)$ (2.24) was used in simulation. Similar distributions of strains and damage parameter are presented in Fig. 2.18.

An analysis of the resulting strain distribution shows that, due to an increase in the rate of accumulation of irreversible strain in the case of cyclic overloads, the level of strain accumulated by the time of failure in the latter case is much higher, by about 20–30%. The maximum strain increases from 1.7 to 2.2%. From the analysis of the distributions, it can be seen that the zones with maximum deformation remain practically the same as in the case of static loading.

The fracture time was changed insignificantly, this was only due to processes of stress varying due to more intensified creep. However, it is possible to stress the expansion of the zones of possible fracture: now it is practically equally likely in both places with maximum damage - both near the fixed side of the blade and in the area of the shelf.

The obtained results cannot be considered completely satisfactory from the point of view of design demands for blades with the necessary long-term strength. The lifetime of 22-24 hours corresponds to approximately the same number of GTE work cycles, which is insufficient. In this regard, we will demonstrate the possibility of making corrections to the model by increasing the thickness of the blade walls by 25%, and the height of the shelf by 15%. The developed FE preprocessor allows you to quickly switch to a new model. Further in the text, we will refer to the model

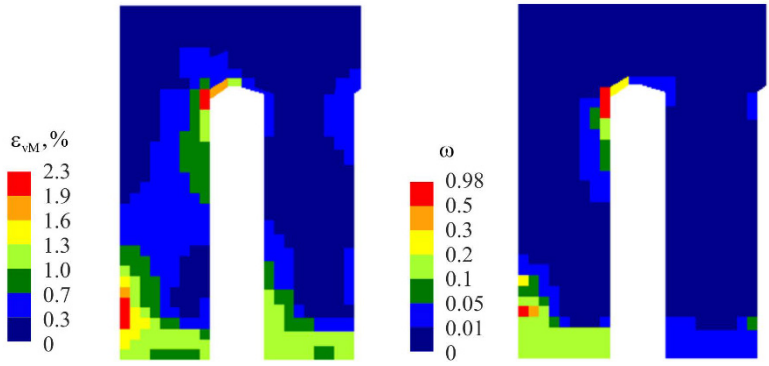

Fig. 2.18: 17 Distribution of the von Mises strain (a) and damage parameter (b), blade made from nickel based alloy (Ni 57%, Cr 16%, Co 11%, W 5%). Model 1, cyclic loading. t = 22.47 h.

considered above as model number 1, and the new one with increased dimensions as model number 2.

For model 2, a similar cycle of calculations was carried out, as presented above for model 1. Additionally, the influence of the pressure level from the gas flow on the deformation and damage in the blade was studied. The value of constant pressure in one of the options was reduced by 4 times, to 3.3 MPa. This version of the calculation model will be given the number 2.2, and the model in which the pressure value of 13 MPa is used will have the number 2.1. Note that due to the increase in the thickness of the walls and the size of the shelf, the overall level of stresses in the problems presented by models 2.1 and 2.2 is 10-15% lower.

The results of the calculations are given in Figs. 2.19-2.22, to model 2.1 a) and 2.2 b), respectively. Figures 2.19 and 2.20 show the distributions of von Mises strains, as well as Figs. 2.21 and 2.22 built for damage parameter distributions. All results are given for time t = 57.1 h, which precedes the moment of completion of hidden fracture.

Based on the analysis of the obtained results, it is possible to draw the following conclusions. The general level of strains remains approximately the same for all three analyzed variants. The maximum values for static load reach 1.6-1.7%, for cyclic loading, when rates are higher, 2.2-2.3%. The same strain level in this particular case is due, most likely, to the compensation of the higher strain rate in model 1 (higher stress level) and twice the time of deformation until the completion of hidden fracture for models 2.1 and 2.2. A significant strain level in all cases occurs in the area of the fixed side. In model 2.1, in which a higher level of pressure is set, during cyclic deformation, a significant strain level, up to 1%, also occurs on the inner side of the first wall. When the lateral pressure decreases (model 2.2), this distribution practically disappears. In general, it is possible to note that the impact of load cyclicity is reflected only on the general increased strain level while preserving the main areas of more intensive deformation.

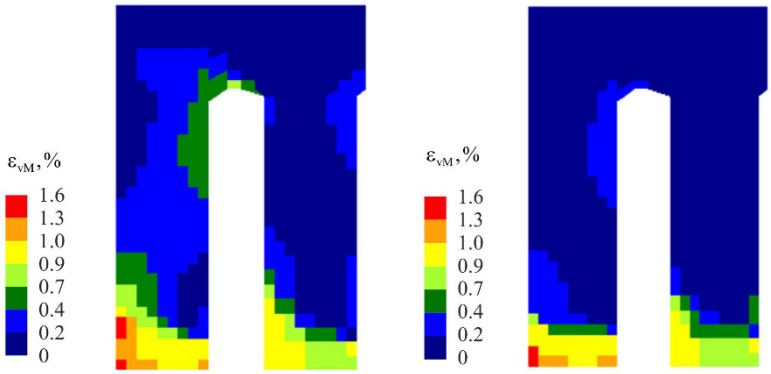

Fig. 2.19: Distribution of the von Mises strain, blade made from nickel based alloy (Ni 57%, Cr 16%, Co 11%, W 5%). Model 2.1 (a) and Model 2.2 (b), static loading. t = 57.1 h.

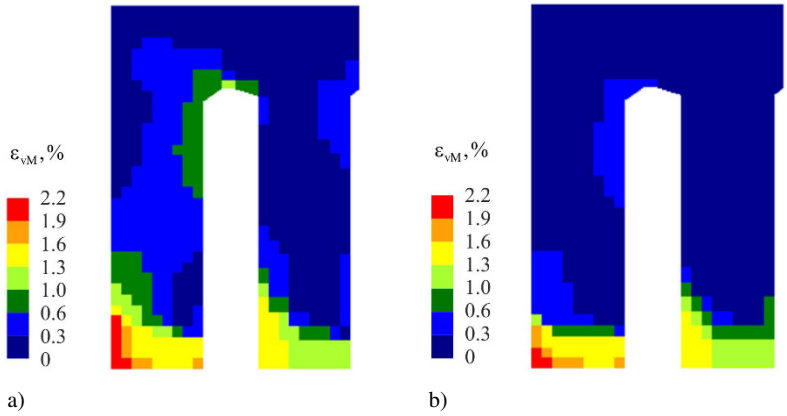

Fig. 2.20: Distribution of the von Mises strain, blade made from nickel based alloy (Ni 57%, Cr 16%, Co 11%, W 5%). Model 2.1 (a) and Model 2.2 (b), cyclic loading. $t = 57.1$ h.

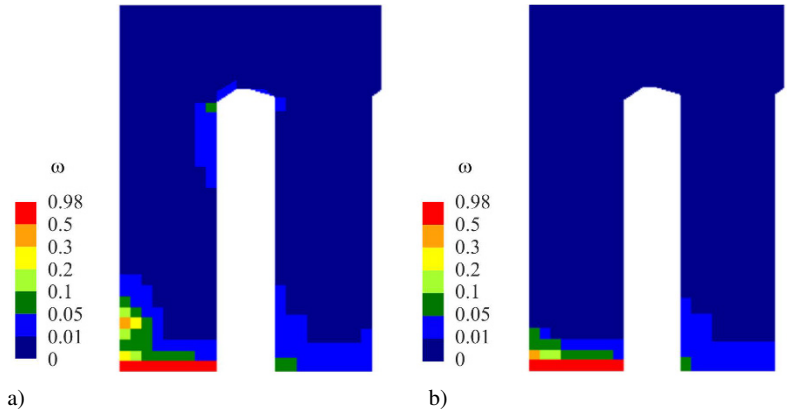

Fig. 2.21: Distribution of the damage parameter, blade made from nickel based alloy (Ni 57%, Cr 16%, Co 11%, W 5%). Model 2.1 (a) and Model 2.2 (b), static loading. $t = 57.1$ h.

When moving from model 1 to model 2, there is a qualitative change in the nature of the place of completion of hidden fracture. In model 2, the failure occurs in the area near fixed side, where the maximum stresses occur under elastic loading. Such a change is due to a decrease in the load on the first wall of the blade, which leads to a lower rate of accumulation of damage. Reducing the pressure on the blade (model 2.2) leads to the fact that practically all the damage is localized in the area of the fixed side.

Due to the non-linearity of the processes of stress redistribution during creep, it is not possible to draw a conclusion about the place of failure in advance, this is determined by the composition of the stress level. With the help of numerical simulation of creep and damage, as shown by the given results, it is possible to make

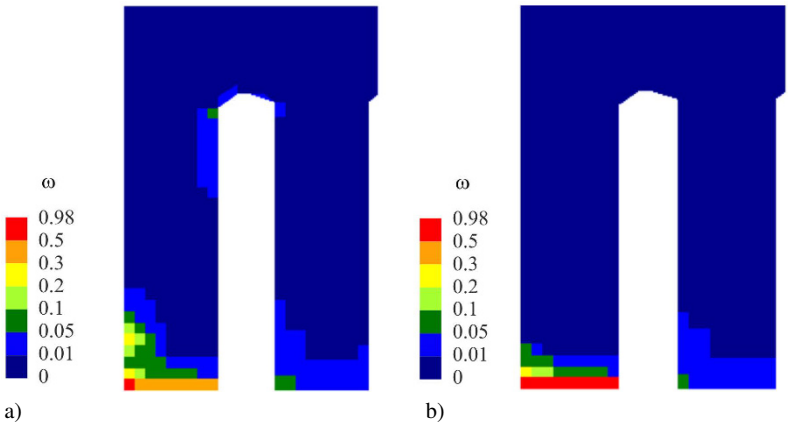

Fig. 2.22: Distribution of the damage parameter, blade made from nickel based alloy (Ni 57%, Cr 16%, Co 11%, W 5%). Model 2.1 (a) and Model 2.2 (b), cyclic loading. $t = 57.1$ h.

such a conclusion. That is, in the case under consideration, even a slight change in the thickness of the blade walls can lead to qualitative changes in the nature of the fracture. Note that the nature of the fracture in model 2, i.e. in the places of transition to the blade root, is more acceptable from the point of view that the real stress level in the three-dimensional model of the blade, which takes into account the contact interaction between the blade and the rotor, will be lower.

2.5.4 Creep Calculations for a Two-dimensional Model of a Blade Made of an Inconel X Alloy

As a second example of the behaviour the considered double-walled blade is creep-damage analysis in more suitable from the point of view of possibility of deformation and fracture occurrence range of temperature-loading conditions. The case of stresses which do not exceed the yield limit is considered. Dimensions are equal to presented for model 2 in previous section.

Blade material is Inconel X alloy, temperature range - 730-830°C. $T_l = 830$°C, $T_{in} = 730$°C, $T_{rmin} = 780$°C. The load is pressure of 0.66 MPa from the gas flow, assumed to be constant over the height of the blade, the action of centrifugal forces with an equivalent intensity that varies linearly from 12 MPa on the outer wall to 8 MPa on the inner wall. The same operations for the stress determining near blade root in 3D statement were done.

For the Inconel X alloy, the creep curves given in [32] were considered at a constant temperature of 1003K and stresses of 168.8 MPa and 211 MPa to determine the Norton creep law material parameters B, n and the long-term strength curve at stresses of 168.8 MPa, 211 MPa and 235 MPa for finding the material damage parameters D, m, l.

For a temperature of 1088 K, curves at the same stress values were used to find the material parameters . After their determining at two different temperatures, them were found for the total temperature range T = 1003 K-1088 K: $B = 1.07 \cdot 10^3 \text{MPa}^{-n}/\text{h}$, $n = 6.33, D = 1.1 \cdot 10^8 \text{MPa}^{-m}/\text{h}, m = 4.86, l = 1.054, Q_c = Q_d = 5.083 \cdot 10^4$ K.

First, we consider the results obtained for the case of a purely static load and temperatures that do not varying over time. The distribution of temperatures in the cross-section of the FE model is presented in Fig. 2.23; von Mises stresses under thermoelastic initial loading: Fig. 2.24; the values of the von Mises strains in this time (a) and damage parameter before the end of the process of hidden damage accumulation (b), $t_* = 61.1$ h: Fig. 2.25.

Next, consider the case of cyclic loading of the blade under consideration, in which the stresses do not exceed the yield limit. In this case, it is possible to apply the constitutive equations obtained using the methods of two time scales and averaging over the period (2.15) when solving the boundary – initial value creep problem (2.33). Let us take for modeling the case with five overloads in a cycle within one hour (Fig. 2.25): $t_1 = 7$ min, $t_2 = t_3 = 5$ min, $T_c = 1$ h. This cycle simulates the operation of a gas turbine for one hour.

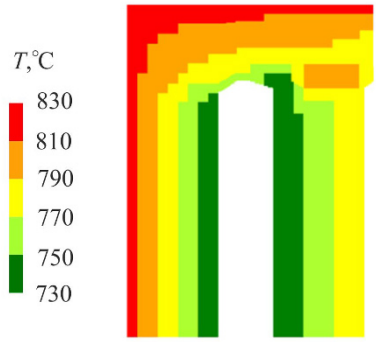

Fig. 2.23 Distribution of temperatures through the cross-section of the FE model, blade made of alloy Inconel X.

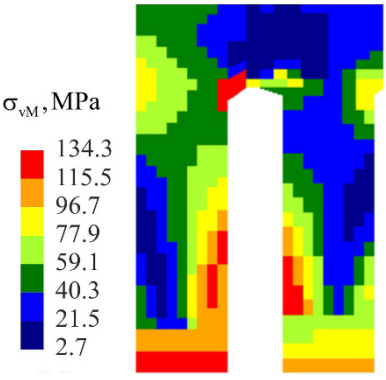

Fig. 2.24 Distribution of von Mises stresses through the cross-section of the FE model, blade made of alloy Inconel X, $t = 0$.

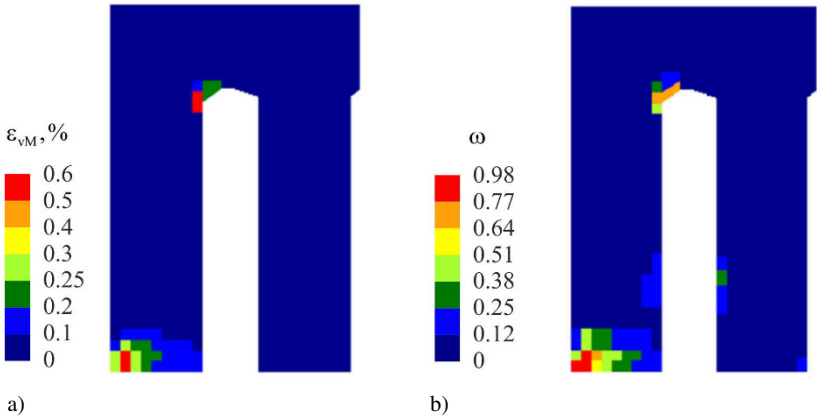

Fig. 2.25: Distribution of von Mises strains a) and damage parameter b) through the cross-section of the FE model, blade made of alloy Inconel X, static loading $t = 61.1$ h.

After performing the transformations and expanding the stress and temperature functions into Fourier series, the expressions for the influence functions of the type included in Eq. (2.15) were obtained:

$$g_n\left(M_k^{\sigma_i}\right) = \int_0^1 \left(a_0\left(M_k^{\sigma_i}\right) + \sum_{k=1}^{\infty} M_k^{\sigma_i} \cos\left(2\pi k\xi\right)\right)^n d\xi, \tag{2.38}$$

$$g_m\left(M_k^{\sigma_e}\right) = \int_0^1 \left(a_0\left(M_k^{\sigma_e}\right) + \sum_{k=1}^{\infty} M_k^{\sigma_e} \cos\left(2\pi k\xi\right)\right)^m d\xi,$$

$$g_T\left(M_k^{T}\right) = \int_0^1 \exp\left(-\frac{Q_c}{T_m}\left(a_0\left(M_k^{T}\right) + \sum_{k=1}^{\infty} M_k^{T} \cos\left(2\pi k\xi\right)\right)^{-1}\right) d\xi,$$

$$M_k^{\sigma_i} = \frac{(\sigma_a)_i}{(\sigma_m)_i}, M_k^{\sigma_e} = \frac{(\sigma_a)_e}{(\sigma_m)_e}, M_k^{T} = \frac{T_a}{T_m},$$

where

$$a_0\left(M_k\right) = \frac{1}{T_p}\left(0.5T_c + \left(5M_k - 2.5\right)t_2 + 2t_3\right),$$

$$a_k\left(M_k\right) = \frac{1}{\pi k}\left[2M_k \sin\left(\frac{\pi k}{T_c}t_2\right) \cdot \left(\cos\left(\frac{\pi k}{T_c}\left(2t_1 + t_2\right)\right) + \right.\right.$$

$$\left. + \cos\left(\frac{\pi k}{T_c}\left(2t_1 + 3t_2 + 2t_3\right)\right) + \cos\left(\frac{\pi k}{T_c}\left(2t_1 + 5t_2 + 4t_3\right)\right) +\right.$$

$$+\cos\left(\frac{\pi k}{T_c}(2t_1+7t_2+6t_3)\right)+\cos\left(\frac{\pi k}{T_c}(2t_1+9t_2+8t_3)\right)\Bigg)+$$
$$+2\sin\left(\frac{\pi k}{T_c}t_3\right)\cdot\left(\cos\left(\frac{\pi k}{T_c}(2t_1+2t_2+t_3)\right)+\cos\left(\frac{\pi k}{T_c}(2t_1+4t_2+3t_3)\right)+\right.$$
$$\left.+\cos\left(\frac{\pi k}{T_c}(2t_1+6t_2+5t_3)\right)+\cos\left(\frac{\pi k}{T_c}(2t_1+8t_2+7t_3)\right)\right)+$$
$$+\frac{1}{t_1}\left(\frac{T_c}{2\pi k}\left(\cos\left(\frac{2\pi k}{T_c}t_1\right)-1\right)+t_1\sin\left(\frac{2\pi k}{T_c}t_1\right)\right)-$$
$$-\frac{1}{T_c-(t_1+5t_2+4t_3)}\left(\frac{T_c}{2\pi k}\left(1-\cos\left(\frac{2\pi k}{T_c}(t_1+5t_2+4t_3)\right)\right)+\right.$$
$$\left.+\ (T_c-(t_1+5t_2+4t_3))\sin\left(\frac{2\pi k}{T_c}(t_1+5t_2+4t_3)\right)\right)\Bigg].$$

The representation of the coefficients a_k does not look very simply, but from a practical point of view, the implementation of constitutive equations with influence functions of the type (2.38) is not a problem: this expression is added to just one small function of the software tool.

Let us consider the results of the calculation analysis of cyclic creep processes, which is accompanied by damage. We consider the case when the pressure on the blade and its heating-cooling occur according to the law presented in Fig. 2.25. The relationship between the components of the stress tensor during additional loading and temperatures during heating is considered to be as follows

$$\sigma_{ij}^a=(1+L)\sigma_{ij}^m,\quad T^a=(1+H)T^m$$

where $L<1, H<1$ are coefficients of the overloading and heating.

First, we present the numerical simulation data for different values of L and $H=0$ m. They are presented in Fig. 2.26 and in Table 2.1. Analyzing the table, we come to the conclusion that the increase in cycle stress values leads to a reduction in the lifetime values and an increase in strains. Similar results were obtained earlier with other cycle parameters [25–28] and simple geometry.

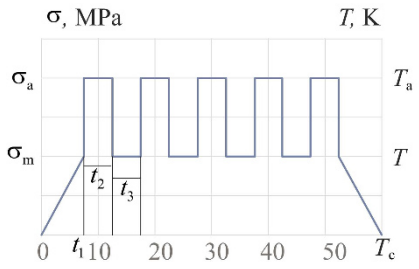

Fig. 2.26 Dependence of stress and temperature from time through the loading cycle.

Table 2.1: Dependence of the time to fracture and maximum von Mises strains on the coefficient of additional loading.

L	0	0.16	0.25	0.33	0.5
Time to fracture, h	0.6	54.95	53.37	51.65	47.88
Maximum von Mises strain,%	1.6	1.2	1.3	1.35	1.4

As an example, Fig. 2.27 shows the distribution of the damage parameter and the von Mises strains at $L = 0.5$ along the cross-section of the blade. For other values of L, the distributions are qualitatively similar.

Finally, we present the results of the numerical simulation taking into account the cyclical varying of both loads and temperatures. As an example, consider the case $L = H = 0.25$. The results are shown in Fig. 2.28, where the distributions of the von Mises strains (a) and the damage parameter (b) along the cross-section of the blade are presented. The time to complete the hidden fracture was 44.45 hours.

Comparing the results of calculations taking into account the cyclical effect of temperatures (Fig. 2.28) and without it (Fig. 2.27) for the same value of load increase in the cycle $L = 0.25$, it is possible to conclude that, despite the fact that the value of the time to completion hidden fracture did not change significantly, only for three hours, in the area of the transition to the shelf, a higher value of the damage parameter was obtained, which may indicate the occurrence of an additional fracture place. The level of damage in the fixed side area changes slightly.

Analyzing the change in the strain level, we see that the additional cyclical varying in temperature increases it almost twice, the maximum values from 1.4% increase to 2.7%. Such a difference between varying in strains and the level of damage can be

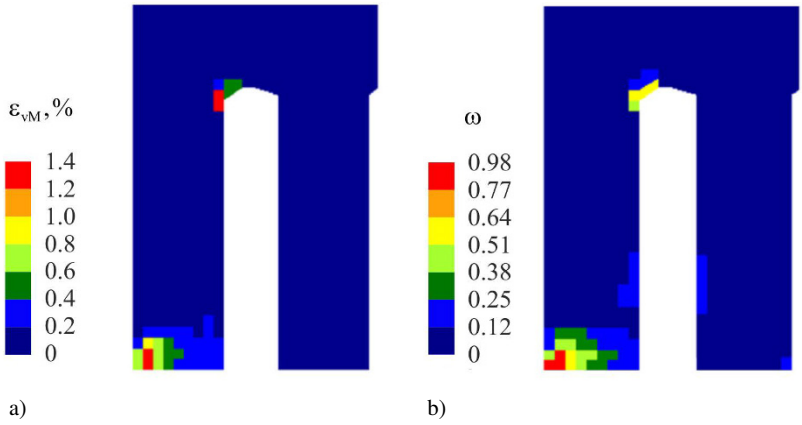

Fig. 2.27: Distribution of von Mises strains a) and damage parameter b) through the cross-section of the FE model, blade made of alloy Inconel X, cyclic loading $t = 47.88$ h.

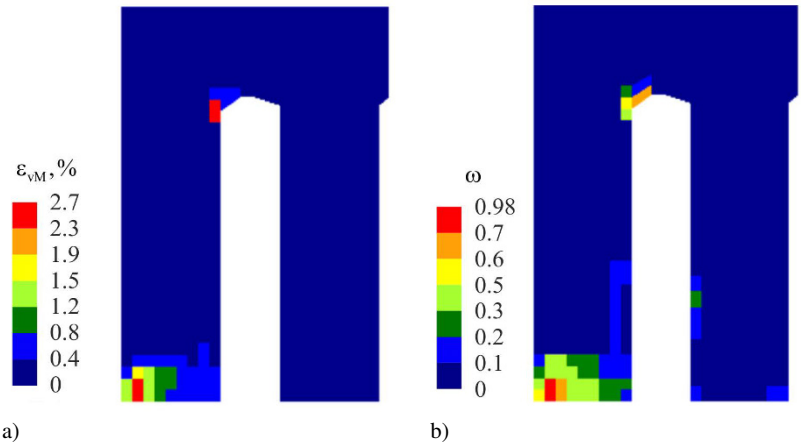

Fig. 2.28: Distribution of von Mises strains a) and damage parameter b) through the cross-section of the FE model, blade made of alloy Inconel X, cyclic loading and heating $t = 44.45$ h.

explained by a greater dependence of the creep rate on stresses for a given material and temperature range than the dependence of the damage parameter on them. This is reflected in the difference of approximately 1.5 times between the values of exponents n and m in the corresponding constitutive equations.

Calculations at other values of L and H provide the corresponding results of the intensification of the level of strains and the reduction of the lifetimes when the values of these coefficients increase.

2.6 Conclusions

An approach to determining the deformation level and long-term strength of structural elements that are under conditions of cyclic loading and heating and in the material of which creep develops is presented. The method for solving the boundary - initial value problems is described. It is based on the traditional combination of FEM and difference methods of integration for initial problems. The basis of the method is the developed and verified constitutive equations for describing the creep and damage of the material. The cases of the cycle stresses varying in a wide range, including the conditions where they exceed the yield stress, as well as the creep when it is not exceeded by stresses, are considered.

The basis of the calculation method is the formulation and description of equivalent creep processes, which allows you to significantly reduce the calculation time due to the absence of the need for direct integration by cycle, which, if there is a sufficiently large number of them, makes it impossible to effectively analyze options during design. Also, cycle integration is a rather complex procedure that cannot ensure

in all cases the convergence of results with average computing resources. Finally, the transition to the modeling of averaged processes provides an opportunity to use modern engineering software complexes, which effectively implement the methods of creep analysis under static loading.

In the case when the cycle stress values do not exceed the yield stress, due to the similarity of the strain and damage accumulation curves under static and cyclic loading, it is possible to apply asymptotic methods together with period averaging and to formulate the form of a new boundary- initial value problem with new averaged constitutive equations. However, in the case of cyclic overloads with exceeding the yield stress, the creep curves under static and cyclic deformation are different. For the latter case, the paper proposes an approach that allows, based on the approximation of cyclic creep curves in a wide range of stresses, to obtain an expression for a new function that reflects the effect of creep acceleration due to load cyclicity.

The proposed approaches and solution methods were used to analyze the creep-damage processes in a model of a GTE blade with double walls. DWTC systems are currently being intensively developed, but due to the complexity of the geometry and significant three-dimensionality of the problem, direct computational analysis of the regularities of long-term high-temperature processes developing in their material is difficult and requires a large amount of resources and time. Due to this, the use of such system‘s models is one of the effective ways to better understand the processes that take place in them.

This paper proposes an approach to construct a simplified model of a blade with double walls, which, on the one hand, takes into account all types of temperature-force influences and stress levels, and on the other hand, thanks to the transition to a two-dimensional scheme, provides the possibility of both rapid modeling and visual displaying the results in one plane. It is clear that in the future it is necessary to move the main conclusions to three-dimensional modeling case.

The main conclusions obtained during numerical modeling can be summarized as follows. As with the analysis of cyclic creep and damage in simpler implementations of the geometry of structural elements obtained earlier [25–28], it was demonstrated that the addition of cyclic loads and temperatures in comparison with the corresponding static process leads to an increase in the rate of creep and damage accumulation, which is reflected by a greater level of accumulated strains and a shorter time to fracture.

The paper demonstrates the possibilities of the proposed approach to the analysis of the stress-strain state and long-term strength, taking into account the impact of load cyclicity by reducing of the problem dimension. It is clear that for a comprehensive analysis of the behavior of such complex systems as the considered double-wall blade, similar studies should be continued to take into consideration other important influencing factors, such as corrosion, multi-cycle fatigue, thermal shock, and others.

Acknowledgements Dmytro Breslavsky acknowledges the support by the Volkswagen Foundation within the programme “Visiting research program for refugee Ukrainian scientists” (Az. 9C184).

References

[1] Bathe KJ (2014) Finite Element Procedures, 2nd edn. Prentice Hall

[2] Murakami S (2012) Continuum Damage Mechanics - A Continuum Mechanics Approach to the Analysis of Damage and Fracture, Solid Mechanics and Its Applications, vol 28. Springer

[3] Naumenko K, Altenbach H (2016) Modeling High Temperature Materials Behavior for Structural Analysis - Part I: Continuum Mechanics Foundations and Constitutive Models, Advanced Structured Materials, vol 28. Springer

[4] Simo JC, Hughes TJR (1998) Computational Inelasticity. Springer, New York

[5] Zienkiewicz OC, Taylor RL, Fox DD (2013) The Finite Element Method for Solid and Structural Mechanics, 7th edn. Butterworth-Heinemann

[6] Murray AV (2019) Advanced gas turbine cooling: double-wall turbine cooling technologies in turbine ngv/blade applications. Phd thesis, University of Oxford, Oxford

[7] Li Z, Wen Z, Pei H, Yue X, Wang P, Ai C, Yue Z (2022) Creep life prediction for a nickel-based single crystal turbine blade. Mechanics of Advanced Materials and Structures **29**(27):6039–6052

[8] Murray AV, Ireland PT, Rawlinson AJ (2017) An integrated conjugate computational approach for evaluating the aerothermal and thermomechanical performance of double-wall effusion cooled systems. In: Turbo Expo: Power for Land, Sea, and Air, American Society of Mechanical Engineers, vol 5B: Heat Transfer, p V05BT22A015

[9] Rezazadeh Reyhani M, Alizadeh M, Fathi A, Khaledi H (2013) Turbine blade temperature calculation and life estimation - a sensitivity analysis. Propulsion and Power Research **2**(2):148–161

[10] Skamniotis C, Cocks AC (2021) 2d and 3d thermoelastic phenomena in double wall transpiration cooling systems for gas turbine blades and hypersonic flight. Aerospace Science and Technology **113**:106,610

[11] Skamniotis C, Cocks AC (2021) Creep-plasticity-fatigue calculations in the design of porous double layers for new transpiration cooling systems. International Journal of Fatigue **151**:106,304

[12] Skamniotis C, Cocks AC (2022) Analytical shakedown, ratchetting and creep solutions for idealized twin-wall blade components subjected to cyclic thermal and centrifugal loading. European Journal of Mechanics - A/Solids **95**:104,652

[13] Wen Z, Liang J, Liu C, Pei H, Wen S, Yue Z (2018) Prediction method for creep life of thin-wall specimen with film cooling holes in ni-based single-crystal superalloy. International Journal of Mechanical Sciences **141**:276–289

[14] Altenbach H, Brünig M (eds) (2015) Inelastic Behavior of Materials and Structures Under Monotonic and Cyclic Loading, Advanced Structured Materials, vol 57. Springer, Cham

[15] Barrett PR, Hassan T (2020) A unified constitutive model in simulating creep strains in addition to fatigue responses of haynes 230. International Journal of Solids and Structures **185-186**:394–409

[16] Chaboche JL, Kanouté P, Azzouz F (2012) Cyclic inelastic constitutive equations and their impact on the fatigue life predictions. International Journal of Plasticity **35**:44–66

[17] Ding B, Ren W, Zhong Y, Yuan X, Zheng T, Shen Z, Guo Y, Li Q, Liu C, Peng J, Brnic J, Gao Y, Liaw PK (2022) Comparison of the creep-fatigue cyclic life saturation effect for three different superalloys. Materials Science and Engineering: A **842**:143,086

[18] Dong Y, Zhu Y, Wu F, Yu C (2022) A dual-scale elasto-viscoplastic constitutive model of metallic materials to describe thermo-mechanically coupled monotonic and cyclic deformations. International Journal of Mechanical Sciences **224**:107,332

[19] Meng L, Chen W (2022) A new thermodynamically based model for creep and cyclic plasticity. International Journal of Mechanical Sciences **214**:106,923

[20] Ohno N, Nakamoto H, Morimatsu Y, Okumura D (2021) Modeling of cyclic hardening and evaluation of plastic strain range in the presence of pre-loading and ratcheting. International Journal of Plasticity **145**:103,074

[21] Wang C, Xuan FZ, Zhao P, Guo SJ (2021) Effect of cyclic loadings on stress relaxation behaviors of 9–12%cr steel at high temperature. Mechanics of Materials **156**:103,787

[22] Zhang W, Wang X, Gong J, Jiang Y, Huang X (2017) Experimental and simulated characterization of creep behavior of p92 steel with prior cyclic loading damage. Journal of Materials Science & Technology **33**(12):1540–1548

[23] Chaboche JL (2002) Damage mechanics. In: Comprehensive Structural Integrity, Pergamon Press, vol 2, pp 213–282

[24] Lemaitre J, Chaboche JL (1994) Mechanics of Solid Materials. Cambridge University Press, Cambridge

[25] Breslavskii DV, Morachkovskii OK (1998) Nonlinear creep and the collapse of flat bodies subjected to high-frequency cyclic loads. International Applied Mechanics **34**(3):287–292

[26] Breslavsky DV, Morachkovsky OK, Tatarinova OA (2008) High-temperature creep and long-term strength of structural elements under cyclic loading. Strength of Materials **40**(5):531–537

[27] Breslavsky D, Morachkovsky O, Tatarinova O (2014) Creep and damage in shells of revolution under cyclic loading and heating. International Journal of Non-Linear Mechanics **66**:87–95

[28] Breslavs'kyi DV, Korytko YM, Morachkovs'kyi OK (2011) Cyclic thermal creep model for the bodies of revolution. Strength of Materials **43**(2):134–143

[29] N RY (1969) Creep Problems in Structural Members. North-Holland Series in Applied Mathematics and Mechanics, North-Holland Publishing Company, Amsterdam

[30] Maksyuta II, Klyass OV, Kvasnitskaya YG, Myalnitsa GF, Mikhnyan EV (2014) Technological features of high chrome nickel allay, complex-alloyed rhenium and tantalum (in Russ.). Electrometallurgy Today (1):41–48

[31] Maugin GA (1999) The Thermomechanics of Nonlinear Irreversible Behaviors - An Introduction, World Scientific Series on Nonlinear Science Series A, vol 27. World Scientific

[32] Guarnieri G (1954) The creep-rupture properties of aircraft sheet alloys subjected to intermittent load and temperature. In: Frey D (ed) Symposium on Effect of Cyclic Heating and Stressing on Metals at Elevated Temperatures ASTM STP No. 165-EB, ASMT, pp 105–147